Hydrogen Production via Steam Reforming of Ethanol on Phyllosilicate-Derived Ni/SiO$_2$: Enhanced Metal−Support Interaction and Catalytic Stability

Chengxi Zhang, Hairong Yue, Zhiqi Huang, Shuirong Li, Gaowei Wu, Xinbin Ma, and Jinlong Gong*

Key Laboratory for Green Chemical Technology of Ministry of Education, School of Chemical Engineering and Technology, Tianjin University, Tianjin 300072, China

Ⓢ *Supporting Information*

ABSTRACT: This paper describes the design of Ni/SiO$_2$ catalysts obtained from a phyllosilicate precursor that possess high activity and stability for bioethanol steam reforming to sustainably produce hydrogen. Sintering of metal particles and carbon deposition are two major issues of nickel-based catalysts for reforming processes, particularly at high temperatures; strong metal−support interaction could be a possible solution. We have successfully synthesized Ni-containing phyllosilicates by an ammonia evaporation method. Temperature programmed reduction results indicate that the metal−support interaction of Ni/SiO$_2$ catalyst prepared by ammonia evaporation method (Ni/SiO$_{2P}$) is stronger due to the unique layered structure compared to that prepared by conventional impregnation (Ni/SiO$_{2I}$). With the phyllosilicate precursor nickel particles highly disperse on the surface, remaining OH groups in the unreduced phyllosilicates promote nickel dispersion and carbon elimination. We also show that high dispersion of Ni and strong metal−support interaction of Ni/SiO$_{2P}$ significantly promote ethanol conversion and H$_2$ production in ethanol steam reforming. Ni/SiO$_{2P}$ produces less carbon deposition compared to Ni/SiO$_{2I}$; for the latter, a surface layer of Ni$_3$C formed during the deactivation.

KEYWORDS: *Ethanol steam reforming, Metal−support interaction, Ni/SiO$_2$, Phyllosilicates, Hydrogen production*
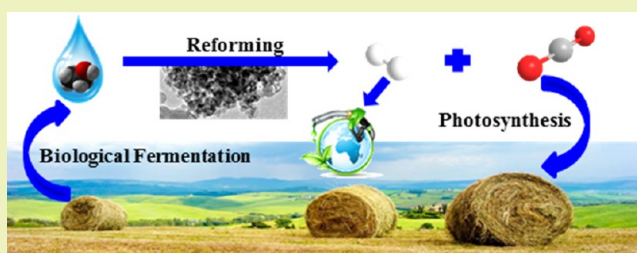
INTRODUCTION

Energy is an indispensable element in our everyday lives. Nowadays most of our energy comes from fossil fuels, a nonrenewable energy source emitting tons of carbon dioxide, which has induced severe greenhouse effects. Meanwhile, the rapid development of society in the 21th century demands a great supply of energy, which leads to a surge in the utilization of fossil fuels and severe pollution of the environment.[1] This spurs the development of green and renewable energy.[2] Production of energy from biomass has the potential to lower greenhouse gas emissions compared to the combustion of fossil fuels, because the CO$_2$ released during energy conversion is consumed during subsequent regrowth of biomass.[3] Among numerous approaches for producing renewable energy from biomass, reforming is a classical and efficient method.[4] Bioethanol steam reforming (ESR) for hydrogen production has attracted much attention since bioethanol is sustainable,[5−7] cheap, easy to handle, low in toxicity, and thermodynamically feasible to decompose.[8] The ESR process can yield a concentration of 60−84% of H$_2$ containing CO, CO$_2$, and CH$_4$ as byproducts.[9] As the products of ESR are mainly hydrogen rich gases, they have been used in conventional internal combustion engines or gas turbine to provide power or heat. However, it would be more desirable to use fuel cells to convert hydrogen energy into electricity efficiently and cleanly.[10] When H$_2$ is applied for fuel cells, the byproducts should be purified by water gas shift and CO preferential oxidation to eliminate CO.[11] The conversion of oxygenated hydrocarbons into hydrogen appears to be advantageous for stationary applications, such as producing hydrogen as a reactant for chemical processes, supplying hydrogen for fuel cells (e.g., a battery charger), or producing hydrogen as a feed to an electrical generator operated using an internal combustion engine.[12]

Investigations on understanding of the nature of ESR catalysts have been burgeoned due to the increasing interests in hydrogen fuel cells. The ESR catalysts mainly include supported base-metals (e.g., Ni, Co, Cu)[13−16] and noble-metals (e.g., Pt, Rh, Ru, Pd, and Ir).[17−19] Although noble-metal-based catalysts exhibit excellent activity and stability in ESR,[10] their large scale application is limited primarily due to the high cost and low reserve of the active metal. Thus, the development of a non-noble catalytic system with desirable activity and stability would be an important step in making the ESR more economically feasible. Among base metals, supported Ni catalysts have been widely examined considering their superior

ability in C−C, C−H, and C−O bond cleavage and dehydrogenation.[10,20−22] High dispersion of nickel nanoparticles is crucial for highly efficient conversion of ethanol and H_2 production since it can provide more sites for C−C and C−H bond activation.[23] However, nickel catalysts suffer from sintering of the metal particles and carbon deposition, which causes the catalyst deactivation and reactor plugging.[24] One possible solution is to engineer catalysts with strong metal−support interaction that could suppress sintering and carbon formation.[25,26]

In order to improve the metal−support interaction, several unconventional structures have been studied, e.g., hydrotalcites and perovskites.[27−31] Urasaki et al. have demonstrated that Ni/LaAlO$_3$ and Ni/SrTiO$_3$ showed high catalytic activities among the Ni/perovskites and longer-term stabilities than the conventional catalyst.[32] However, these materials usually has a relatively small specific surface area.[33] The application of novel preparation routes to produce silica-based catalysts has been reported to enhance metal−support interaction, particularly for silica supported Ni catalysts.[34−36] Che et al.[35] reported a two-step procedure for the preparation of Ni/SiO$_2$ (2:1 nickel phyllosilicates (PS)) catalysts exhibiting enhanced interaction between Ni and SiO$_2$. It has also been reported that the PS phases formed have a strong interaction with Ni species due to the layered PS structure.[37,38] The silica supported nickel materials prepared by deposition−precipitation and ion exchange methods possess considerable amount of PS phases.[37,39] Two types of Ni-containing PS are typically obtainable with different Ni to PS molar ratios (i.e., 2:1 and 1:1). The 2:1 Ni−PS (i.e., Ni$_3$Si$_4$O$_{12}$H$_2$) contains about ∼36 wt % Ni, whereas the other one has a formula of Ni$_3$Si$_2$O$_9$H$_4$ with ∼46 wt % Ni. The model structures of both components are shown in Scheme 1. In Ni 1:1 PS, each layer consists of one

Scheme 1. Structure of Ni-Containing PS

1:1 PS   2:1 PS
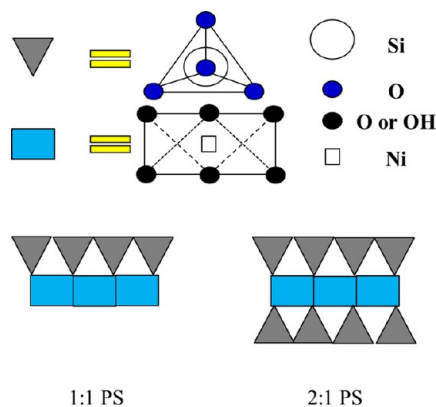
tetrahedral sheet (Si coordinated to four oxygen atoms) and one octahedral sheet (Ni coordinated to six oxygen atoms or hydroxyl groups). In the case of a 2:1 PS layer structure, one octahedral sheet sandwiched between two tetrahedral sheets.

This paper describes the synthesis, characterization, and utilization of Ni/SiO$_2$ catalysts for the steam reforming of ethanol. Ni-containing PS was prepared by the ammonia evaporation (AE) method as a catalyst precursor, and the reduced catalyst (denoted as Ni/SiO$_{2P}$) was compared with that prepared by the conventional impregnation (denoted as Ni/SiO$_{2I}$) in ESR at 400−700 °C. X-ray diffraction (XRD), transmission electron microscopy (TEM), and infrared (IR)

were used to characterize the structure and morphology of Ni-containing PS; BET, temperature programmed reduction (TPR), XRD, and TEM were used to characterize the textural properties and nature of the metal−support interaction, crystalline phase, and nickel dispersion of the catalyst. We had also performed the stability test at 400 and 600 °C to understand the cause of differences in stability of the catalysts.

■ EXPERIMENTAL SECTION

Preparation of Ni/SiO$_{2P}$ Catalyst. Ni/SiO$_{2P}$ powder was prepared by the AE method described briefly as follows. A certain amount of Ni(NO$_3$)$_2$·3H$_2$O and a 25 wt % ammonia aqueous solution (NH$_3$/Ni molar ratio = 8) dissolved in deionized water were mixed and stirred for 10 min. Silica sol (Qingdao Yurui chemical Co., Ltd. SiO$_2$ content, 30 wt %; viscosity, 7.0 mPa·s; density, 1.19−1.21 g/cm^3; average particle size, 10−20 nm) was then added to the nickel ammonia complex solution and stirred for 6 h. The initial pH of the suspension was 11−12. All the above operations were performed at room temperature. The suspension was heated in a water bath preheated to 80 °C to allow for the evaporation of ammonia, the decrease of pH, and the consequent deposition of nickel species on silica. When the pH value of the suspension decreased to 6−7, the evaporation process was terminated. The resultant precipitate was then filtered and washed thoroughly with deionized water to remove the residual ammonium ions. Then, the solid was dried at 80 °C for 12 h in a vacuum drying oven and was calcined at 700 °C for 4 h in a muffle furnace. Although pure phyllosilicate has 36 wt % of nickel, for comparison purposes, the reference catalyst prepared by the impregnation method typically has lower Ni loading. Therefore, we fixed the amount of Ni loading to 20 wt %, which is nearly equal to those used in reforming reactions industrially. For this loading of the Ni/SiO$_{2P}$ catalyst, phyllosilicate is embedded in the silica matrix.

Preparation of Ni/SiO$_{2I}$ Catalyst. Commercial SiO$_2$ (Qingdao Yurui chemical Co., LTD) was calcined at 700 °C for 2 h. Ni/SiO$_{2I}$ was prepared by the incipient wetness impregnation method. SiO$_2$ was impregnated in a Ni(NO$_3$)$_2$·6H$_2$O aqueous solutions by mechanical agitation at 50 °C for 12 h, followed by evaporated at 60 °C using vacuum rotary until the ethanol was removed. The resultant solid was dried at 100 °C for 12 h and, then, calcined at 700 °C for 2 h. The amount of Ni loading was fixed to 20 wt %.

Activity Test. Catalytic tests were conducted at the atmospheric pressure in a quartz fixed-bed reactor (Φ 10 × 30 mm) loaded with 0.1 g catalysts (20−40 mesh) mixed with 1 mL of quartz particles. Prior to the test, the catalysts were reduced at 700 °C online for 1 h in a flow of 10 vol % H$_2$/N$_2$ (50 mL/min). The liquid solution with a water/ethanol molar ratio of 8 (i.e., S/C = 4) was fed at 0.066 (reactivity test at different temperatures and 400 °C stability)/0.02 (600 °C stability) mL/min through an HPLC pump into a heated chamber (150 °C) to evaporate the solution completely in the stream of N$_2$ (60 mL/min). The products were analyzed online by two gas chromatographs. One is equipped with a flame ionization detector (FID) and a Porapak-Q column with N$_2$ as a carrier gas to analyze the organic species such as ethanol and methane. The other one is integrated with a thermal conductivity detector (TCD) and a TDX-01 column using He as a carrier gas to monitor the incondensable gas species including hydrogen, carbon dioxide, carbon monoxide, and methane.

Characterization. BET surface areas and pore structure of catalysts were measured using a Micromeritics Tristar 3000 analyzer by nitrogen adsorption at −196 °C. The specific surface areas were calculated from the isotherms using the BET method, and the pore distribution and the cumulative volumes of pores were obtained by the BJH method from the desorption branches of the adsorption isotherms.

X-ray diffraction patterns were recorded with a Bruker D8 Focus operated at 40 kV and 40 mA equipped with nickel-filtered Cu Kα radiation (λ = 1.54056 Å) and a 2θ value ranging from 15 to 85° (or 5 to 65°) at a scanning rate of 0.02°/step and 0.15 s/step.

IR spectra were recorded on a Thermo Nicolet 6700 spectrometer equipped with a deuterated triglycine sulfate (DTGS) detector. The

Table 1. Textural Properties of Ni/SiO₂ Catalysts

sample	BET surface area (m²/g)	average pore diameter (Å)	pore volume (cm³/g)	H₂ consumed in TPR/in reduction conditions (cm³/g)	reduction extent (%)[a]	particle size (nm)[b]	crystal size (nm)[c]	S_{Ni} m²/g$_{Ni}$[d]
commercial SiO₂	428	36.9	0.41					
Ni/SiO₂P	384	123.9	1.33	65.6/60.5	92	3.3/5.8/5.7	—/4.0/5.8	14.6/9.4
Ni/SiO₂I	328	36.0	0.25	60.0/59.6	99	20.4/10.1/12.0	20.0/10.0/12.4	9.4/5.4

[a]Determined from the amount of H₂ consumed in TPR divided by that consumed in reduction conditions. [b]Determined from TEM graph (statistics on 100 particles randomly picked up from TEM images), (before reaction/after 400 °C reaction/after 600 °C reaction). [c]Ni crystal size determined by the Scherrer equation from the (111) plane of Ni in XRD patterns (before reaction/after 400 °C reaction/after 600 °C reaction). [d]Nickel active surface area determined by H₂ pulse chemisorption, (before reaction/after 400 °C reaction)
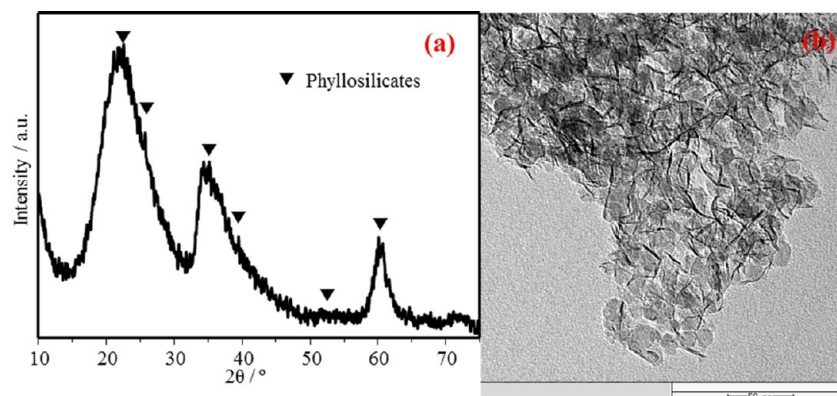

Figure 1. XRD patterns (a) and TEM images (b) of Ni-containing PS.

samples were finely grounded, dispersed in KBr, pelletized, and dried. The spectral resolution was 4 cm⁻¹, and 32 scans were recorded for each spectrum.

TEM images were obtained on a FEI Tecnai G2 F20 transmission electron microscope at 100 kV. The sample powder was dispersed in ethanol by sonification; drops of the suspension were applied onto a copper grid-supported transparent carbon foil and dried in air.

Nickel active surface area was determined by H₂ pulse chemisorption (Micromeritics AUTOCHEM II 2920). After the catalyst was reduced at 700 °C for 1.0 h under 10% H₂/Ar flow, it was cooled down to room temperature under Ar, and then H₂ pulses were injected until the eluted peak area of consecutive pulses was constant. The active surface area of Ni was calculated from the volume of H₂ adsorbed by assuming a H/Ni$_s$ (surface nickel atom) stoichiometry of 1 and a surface area of 6.5×10^{-20} m² per Ni atom.[40]

Temperature programmed reaction spectroscopy (TPRS) experiments were carried out in a flow reactor (Φ 4 × 10 mm) connected to a QIC 20 HIDEN quadrupole mass spectrometer. Prior to any experiments, all samples were reduced in situ using a flow of 10 vol % H₂/Ar (30 mL/min). After purging with Ar for 15 min, the sample (20−40 mesh) was cooled under Ar to room temperature (20 °C). A mixture containing 0.3% EtOH and 2.4% H₂O in Ar was directed through the catalyst bed at a rate of 30 mL/min while temperature was ramped from 20 to 800 °C with a linear rate of 10 °C/min. The reactor effluent was continuously monitored by the mass spectrometer and gas-phase composition was calculated from the mass spectrometer signal at m/e ratios of 44, 40, 31, 28, 15, and 2 for CO₂, Ar, CH₃CH₂OH, CO, CH₄, and H₂, respectively.

Carbon deposition analysis was carried out using a thermal analysis system (STA449F3, NETZSCH Corp.). The experiments were performed in a flow of air (50 mL/min) with a heating rate of 10 °C/min and a final temperature of 800 °C.

Conversion, selectivity, and yield calculations:

$$X_{EtOH} = \frac{F_{EtOH,in} - F_{EtOH,out}}{F_{EtOH,in}} \times 100\%$$

$$H_2 \text{ selectivity } (\%) = [(\text{moles of } H_2 \text{ produced})$$
$$\times 2/(\text{moles of H atom in gas products})]$$
$$\times 100$$

$$S_j = 100 \times [(\%j \times i)]/[(\%CO + (\%CO_2) + (\%CH_4)$$
$$+ 2(\%C_2H_4) + 2(\%C_2H_6) + 2(\%CH_3CHO)$$
$$+ 3(\%CH_3COCH_3))]$$

where j represents the carbon containing species in the products, including CO, CO₂, CH₄, C₂H₄, C₂H₆, CH₃CHO, and CH₃COCH₃. i is the number of carbon atoms in the carbon-containing species.

TOF = mole flow rate of ethanol converted (at initial stable time, within 10 h)/mol of the active nickel (calculation based on the result of H₂ pulse chemisorption before reaction) in the catalyst

The carbon balance was within ±5% for all catalytic runs. Data for the catalyst activity were collected when the reaction reached stable conditions, and repeated tests have been run to confirm the activity. It should be emphasized that according to the definitions, the sum of the selectivities of H₂ and the carbon-containing species does not lead to unity since they are calculated based on independent hydrogen and carbon balances, respectively.

■ RESULTS

Characterization of the Calcined Ni/SiO₂ Catalysts. The N₂ adsorption−desorption isotherms of the Ni/SiO₂ samples and their pore size distribution curves are illustrated in Supporting Information Figure S1. Textural properties of the catalysts are summarized in Table 1. The BET surface area of Ni/SiO₂I catalyst decreases slightly after impregnation. The Ni/SiO₂P possesses larger BET surface area, pore volume, and average pore diameter than Ni/SiO₂I. The pore shape of Ni/SiO₂P is "slitlike", whereas that of Ni/SiO₂I is "spherical" (Supporting Information Figure S1A). The pore size distribution curves derived from the desorption branch using

the BJH algorithm (Supporting Information Figure S1B) show that they are both mesoporous. The pore size of Ni/SiO_{2I} is in the range of 2−8 nm compared to 2−40 nm for Ni/SiO_{2P}.

XRD patterns of Ni-containing PS are presented in Figure 1a. Diffraction peaks at 5.8°, 19.4°, 26.7°, 33.7°, 39.7°, 53.2°, and 60.9° are attributed to the (001), (100), (103), (110), (200), (210), and (300) facets of 2:1 PS, respectively.[41,42] Figure 1b illustrates the TEM images of Ni-containing PS, confirming the formation of characteristic layered structures of Ni-containing PS.

IR spectra of Ni/SiO_2 catalysts are shown in Figure 2. The vibration bands at 460 and 800 cm^{-1} are attributed to the Ni−
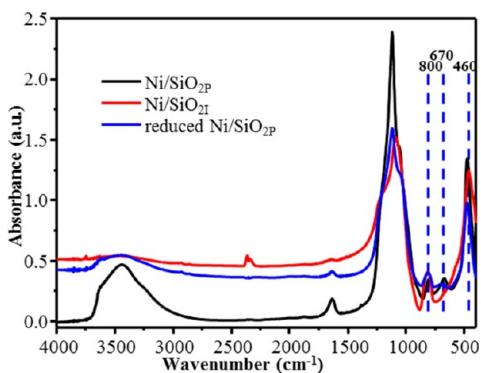

Figure 2. IR spectra of Ni/SiO_2 catalysts.

O−Si vibrations and the tetrahedral Si−O mode vibrations,[41] respectively, which appeared in both Ni/SiO_2 catalysts. The vibration band at ~670 cm^{-1} ascribed to the δOH vibration[43] is observed for Ni/SiO_{2P}, characteristic of the well-formed PS structure.

Characterization of the Reduced Catalysts. TPR profiles of the Ni/SiO_2 catalysts are shown in Figure 3a. The reduction peak at ~360 °C can be ascribed to the reduction of NiO particles.[44] The reduction peak at 500 °C is attributed to the isolated Ni^{2+} ions grafted to surface groups from silica, while Ni^{2+} ions in bulk phyllosilicates are reduced at 550−900 °C, depending on the crystallinity.[45] The main reduction peak of Ni/SiO_{2P} at higher temperature compared to Ni/SiO_{2I}, indicate a stronger metal−support interaction of Ni-containing PS.[34] The reduction extent of the Ni/SiO_2 catalysts is shown in Table 1. The reduction extent of Ni/SiO_{2P} is 92%, while that of Ni/SiO_{2I} is 99%.

Upon reduction, Ni/SiO_{2I} possesses good nickel crystallinity, and the crystal size of Ni particles is ~20 nm calculated by the Scherrer equation from the Ni(111) plane (Figure 3b). Comparatively, Ni-containing PS phase is still present in the XRD patterns of Ni/SiO_{2P} and the Ni peak is very weak, implying fine dispersion of Ni species on the support. The improved dispersion of Ni in Ni/SiO_{2P} over Ni/SiO_{2I} is in accordance with the result of H$_2$-chemisorption.

TEM micrographs of the Ni/SiO_2 catalysts upon reduction are shown in Figure 4. Clearly, spherical nickel particles are well dispersed on Ni/SiO_{2P}, while the nickel particles have a wide size distribution on Ni/SiO_{2I}, implying that Ni/SiO_{2P} has a better dispersion over Ni/SiO_{2I}. There was the PS structure remained in Ni/SiO_{2P} (Figure 4a), implying that nickel was not fully reduced after 1 h reduction at 700 °C. The δOH vibration and OH stretching vibration peaks were also observed for Ni/SiO_{2P} upon reduction but with less intensity (Figure 2), suggesting that the PS structure is partly broken down. This is in accordance with TPR results and earlier work that Ni-containing PS cannot be fully reduced when reduction temperatures is lower than 700 °C.[41,46] Nickel particles in Ni/SiO_{2P} have a much smaller mean particle size (~3.3 nm) compared to Ni/SiO_{2I} (~20.4 nm), consistent with the results obtained from the XRD spectra. The difference in particle size could be due to the stronger metal−support interaction in Ni-containing PS that also leads to high dispersion of nickel particles.

Activity and Stability Test of Ni/SiO_2 Catalysts. Figure 5 illustrates ESR reactivity on Ni/SiO_2 catalysts at different temperatures. For a fixed catalyst, TOF of ethanol increases with temperature. TOF of ethanol and H$_2$ selectivity on Ni/SiO_{2P} is higher than that of Ni/SiO_{2I} at low temperatures (e.g., 400 °C). Notably, H$_2$ selectivity first increases with an increase in temperature to 600 °C, and then decreases upon further increasing temperature. Here, ethanol conversions were all lower than 100%, and for a fixed space velocity, ethanol conversion increases with temperature. For a fixed reaction temperature (e.g., 500 °C), CH$_3$CHO selectivity on Ni/SiO_{2P} is lower than that on Ni/SiO_{2I}, indicating a higher C−C bond cleavage reactivity of Ni/SiO_{2P}; wherever CO selectivity on Ni/SiO_{2P} is lower than that on Ni/SiO_{2I}, CH$_4$ and CO$_2$ selectivity on Ni/SiO_{2P} is higher than that on Ni/SiO_{2I}, which implies that water gas shift reaction (WGSR) and methanation activity on Ni/SiO_{2P} is higher. This could be owing to the high surface area of active nickel species of Ni/SiO_{2P}.[23,47,48]
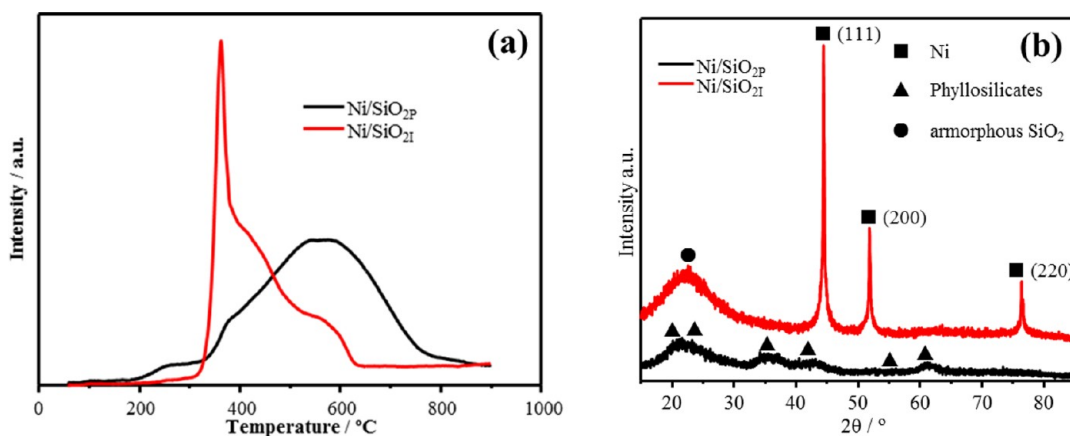

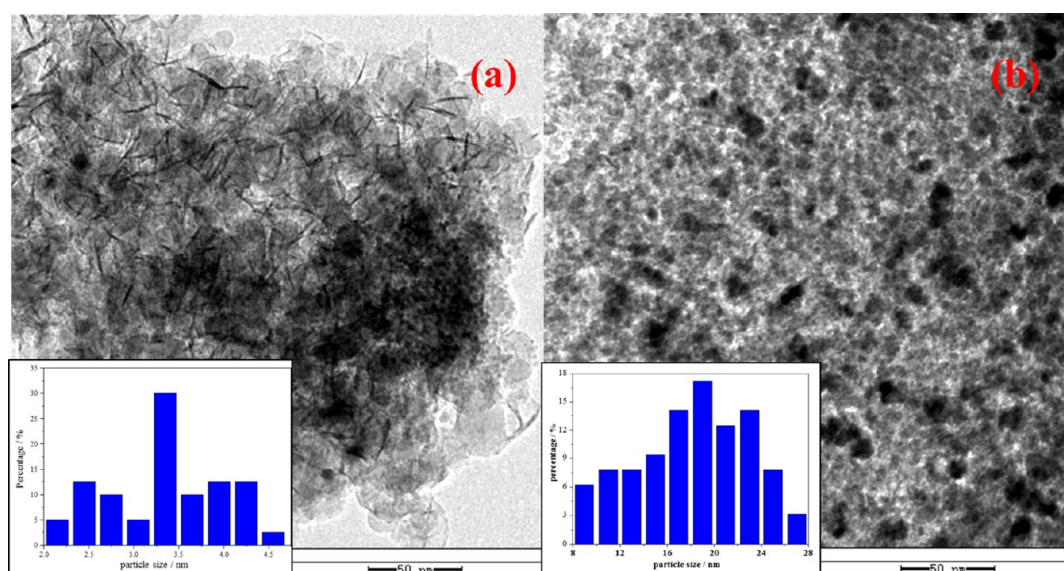**Figure 3.** TPR profiles (a) and XRD patterns (b) of Ni/SiO_2 catalysts upon reduction.

Figure 4. TEM images of Ni/SiO$_2$ catalysts after reduction: (a) Ni/SiO$_{2P}$, (b) Ni/SiO$_{2I}$. Insets are the size distribution of nickel particles.
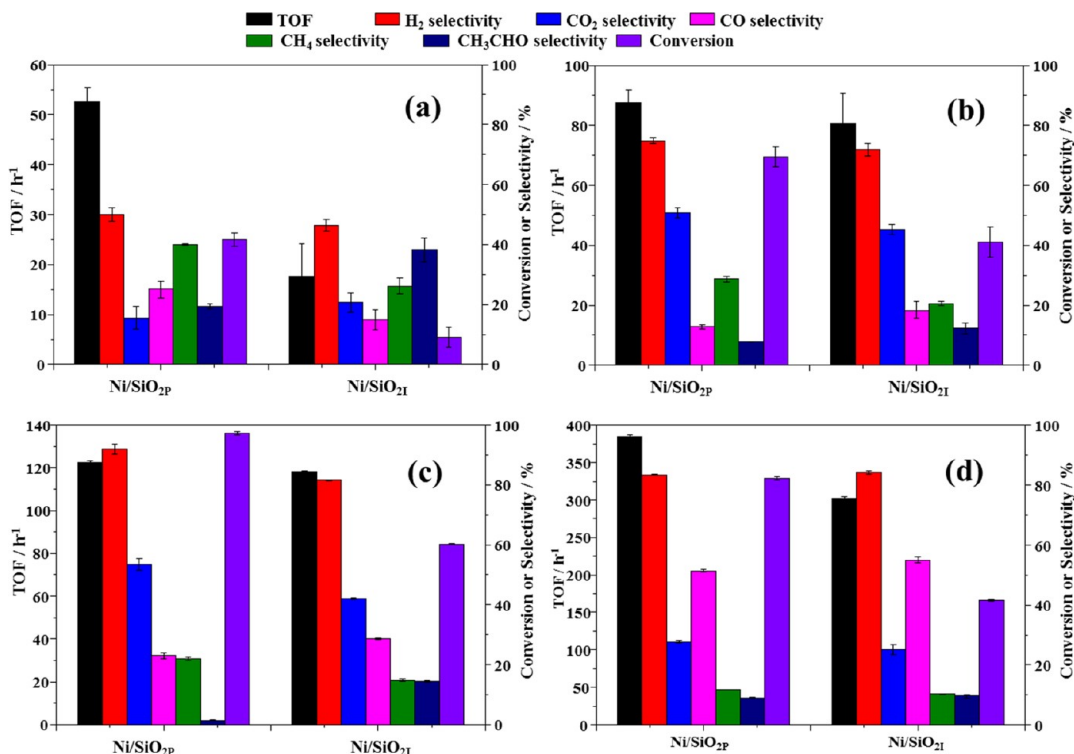

Figure 5. ESR reactivity on Ni/SiO$_2$ catalysts at 400 (a), 500 (b), 600 (c), and 700 °C (d). Reaction conditions: ethanol feed velocity, 2.5 g·h/mol for 600, 500, and 400 °C, 0.82 g·h/mol for 700 °C; 6 vol% of ethanol in gas; S/C = 4, 1 atm.

The stability of the Ni/SiO$_2$ catalysts were tested at 400 and 600 °C, and results are shown in Figure 6. When the reaction was carried out at high space velocities and 400 °C, ethanol conversion on Ni/SiO$_{2P}$ keeps at ∼80% after 30 h reaction, and H$_2$ selectivity keeps nearly intact, indicating the good stability of Ni/SiO$_{2P}$. Comparatively, Ni/SiO$_{2I}$ suffers severe deactivation with ethanol conversion decreasing from 100% to ∼40% after 30 h reaction and selectivity of C2−C3 compounds (e.g., CH$_3$CHO, CH$_3$COCH$_3$) increasing to ∼20%. We also note that selectivity of H$_2$ and CO$_2$ increases slightly after 15 h accompanying with a decrease in CO selectivity, probably due to the fact that WGSR is more efficiently at low ethanol conversions. When the ethanol conversion was low, less carbon containing products were produced and thus more active sites remained for WGSR.[49,50] Since both catalysts deactivate, the catalyst is not very suitable in ESR at 400 °C. However, at 600 °C, Ni/SiO$_{2P}$ shows full ethanol conversion without a significant change in the product distribution during the entire 60 h testing period, while ethanol was partially converted after 40 h reaction on Ni/SiO$_{2I}$, which gradually decreased to ∼90%. CH$_3$CHO was also produced after 55 h reaction.

Characterization of Used Ni/SiO$_2$ Catalysts. Figure 7 shows the XRD patterns of Ni/SiO$_2$ catalysts after the stability test. Nickel, amorphous SiO$_2$, and quartz phases all appear in
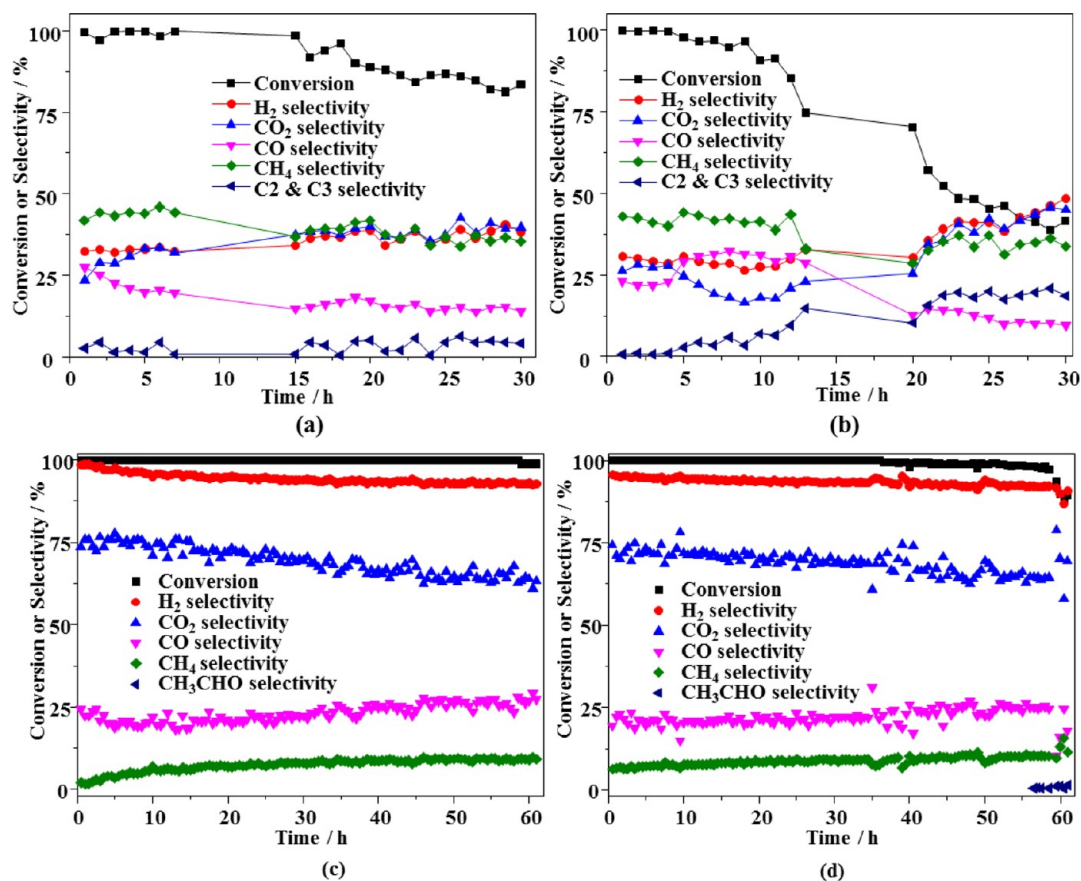
Figure 6. Stability test on Ni/SiO_2 catalysts for (a and c) Ni/SiO_{2P} and (b and d) Ni/SiO_{2I}. Reaction conditions: (a and b) 400 °C, (c and d) 600 °C; 1 atm, ethanol feed velocity, 10 g·h/mol, ethanol in feed, 6 vol % for 400 °C reaction; ethanol feed velocity, 16.4 g·h/mol, ethanol in feed, 3 vol% for 600 °C.
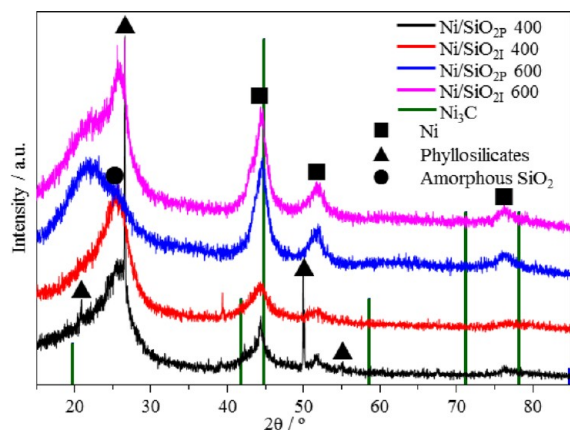
**Figure 7.** XRD patterns of Ni/SiO_2 catalysts upon stability test.

both Ni/SiO_2 catalysts. Surprisingly, the crystal size of nickel of Ni/SiO_{2I} decreases to ~10.0 and ~12.4 nm after the reaction, whereas that of Ni/SiO_{2P} slightly increases. Ni/SiO_{2P} remains its platelike structure, and the nickel particle size increases to ~5.8 and ~5.7 nm after the 400 (Figure 8) and 600 °C (Figure 9) tests, which is in accordance with our XRD results. However, for Ni/SiO_{2I}, nickel particles were enveloped by either amorphous carbon or graphite upon the reaction, and the particle size of nickel decreased to about 10.1 and 12.0 nm after 400 and 600 °C test, respectively. This could be due to the formation of nickel carbide species from severe carbon deposition, which further induces particle reconstruction and

breakdown large nickel particles into smaller ones.[51] But this is not a proof that Ni/SiO_{2I} has the capacity of antisintering, since it has severe carbon deposition surround the nickel particle. However, since Ni_3C and metallic Ni have similar diffraction peaks (as shown in Figure 7), it is not very likely to clearly distinguish the formation of Ni_3C via XRD patterns.

In order to further clarify the cause for the decreased nickel particle size and the severe deactivation on Ni/SiO_{2I}, HRTEM images have been carried out as shown in Figure 8c and d and Figure 9c and d. Indeed, Ni_3C species are around nickel particles on Ni/SiO_{2I}, whereas nickel particles were still well-dispersed on Ni/SiO_{2P}. It is very likely that the strong metal–support interaction between Ni and PS resists Ni_3C formation.[52] Ni_3C has been reported to form in reactions involved hydrocarbons, e.g., methanation and steam reforming.[53,54] Alstrup[51] has proposed a model for carbon filament growth on supported nickel catalysts, in which nickel carbide formed first and would induce the particle reconstruction and severe carbon deposition. In our reaction conditions, Ni_3C formation decreased nickel particle size through the nickel particle reconstruction.

Carbon deposition after stability test was also determined by TGA measurements (as shown in Supporting Information Figure S2 and Figure 10). Carbon deposition rate was calculated from weight loss of catalyst after temperature programmed oxidation divided by catalyst weight and reaction time. The carbon deposition on Ni/SiO_{2I} is more severe compared to Ni/SiO_{2P}, which is in accordance with TEM results. While the carbon formed after 400 °C test was whisker-
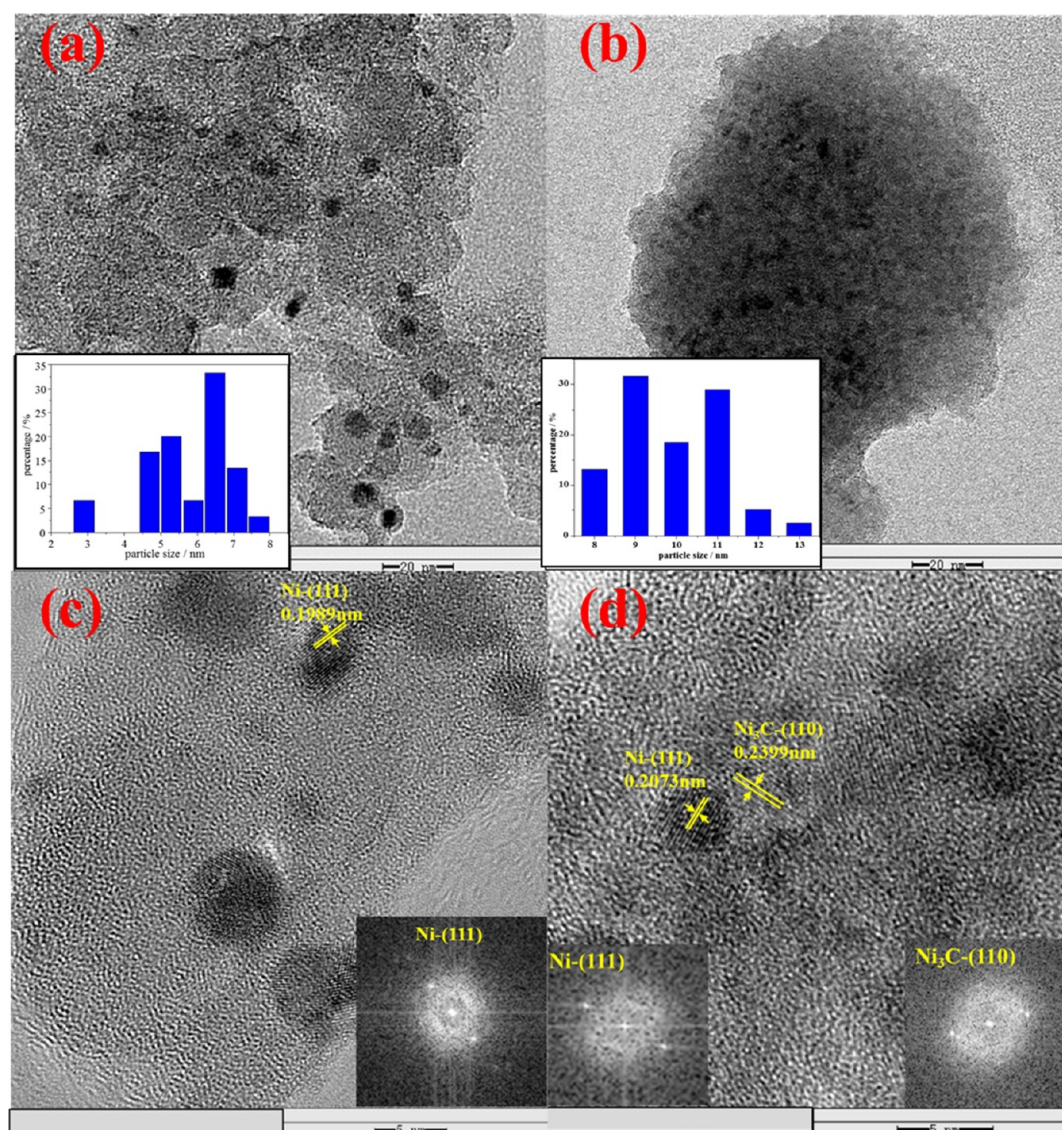
Figure 8. TEM characterization of Ni/SiO$_2$ catalysts after 400 °C stability test (a and b) TEM images and (c and d) HRTEM images for (a and c) Ni/SiO$_{2P}$ and (b and d) Ni/SiO$_{2I}$. Insets are for statistics of Ni particle size.

like carbon (DTG weight loss peak lower than 600 °C), the 600 °C test led to the formation of graphite species, confirmed by DTG results (Supporting Information Figure S2).[52,55] Carbon deposition is mainly induced by methane decomposition on our catalysts; considering high methane concentration and feed velocity of ethanol at 400 °C compared to that at 600 °C, an increased amount of carbon deposition at 400 °C was observed.

■ DISCUSSION

Formation of Ni-Containing PS. Ni-containing PS, also called pimelite or nepouite, is a kind of nickel silicate with a lamellar structure that consists of layers of SiO$_4$ tetrahedral sandwiched between discontinuous layers of octahedral nickel hydroxide. Ni-containing PS is known to form during the preparation of Ni/SiO$_2$ catalysts by the deposition−precipitation method using urea hydrolysis[43] and by hydrothermal synthesis.[46] Our work showed that Ni-containing PS can also be formed using the AE method. Consistent with the earlier work by Kermarec et al.,[39] we have shown that Ni/SiO$_{2P}$ has a larger BET surface area compared to Ni/SiO$_{2I}$ and that the

formation of Ni-containing PS is also corroborated by IR and XRD results. TEM images showed that the filandrous structure characteristic of Ni-containing PS clearly appeared in Ni/SiO$_{2P}$. Therefore, the change in the pore shape from "spherical" to "slitlike" and the increase in the average pore size can be attributed to the formation of a new pore system arising from the filandrous PS structure in Ni/SiO$_{2P}$.

Nickel Species and Properties of the Reduced Ni/SiO$_2$ Catalysts. It has been reported that the nickel particle size depends on the precursor reducibility; poor reducibility leads to small nickel particles.[37,56,57] This phenomenon also applied to our system; that is, the smaller nickel particle size of Ni/SiO$_{2P}$ is consistent with lower reducibility of Ni-containing PS due to the enhanced binding of Ni species with the support. From TEM images of the catalysts upon reduction, one can see that the PS structure remains in Ni/SiO$_{2P}$, implying that there are both octahedral nickel hydroxide and Ni^0 in the structure; whereas only metallic Ni species was detected in Ni/SiO$_{2I}$ based on XRD and TEM results. The differences in metal particle size could be due to the varied particle size of the NiO intermediates (i.e., NiO particles in the unreduced catalyst
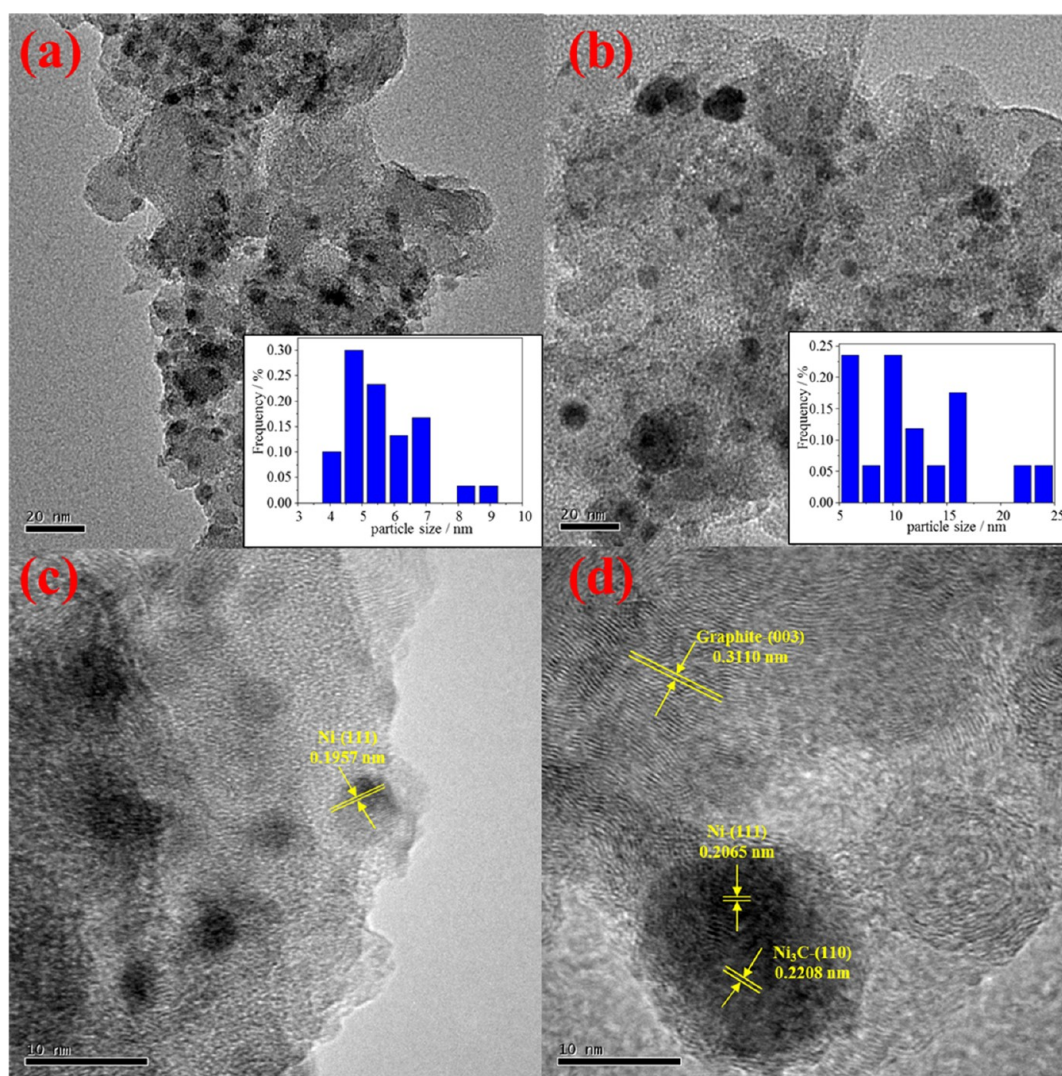
Figure 9. TEM characterization of Ni/SiO$_2$ catalysts after 600 °C stability test (a and b) TEM images and (c and d) HRTEM images for (a and c) Ni/SiO$_{2P}$ and (b and d) Ni/SiO$_{2I}$. Insets are for statistics of Ni particle size.
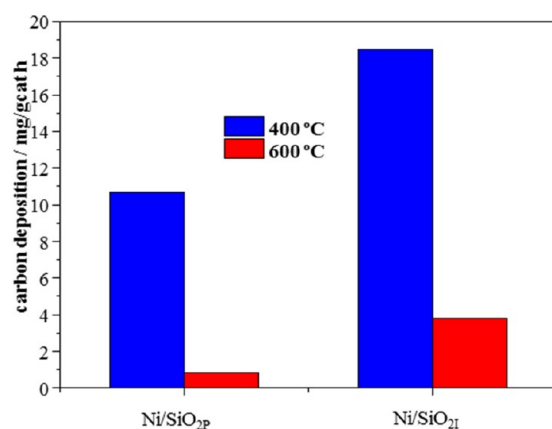

Figure 10. Carbon deposition on Ni/SiO$_2$ catalysts after stability test.

precursor). Indeed, it has been reported that NiO from decomposition of nickel PS is smaller than that from Ni(NO$_3$)$_2$,[37] which is owing to the abundant surface OH groups in PS.[58]

The OH groups in octahedral nickel hydroxide also has important role on carbon resistance. It has been reported that the presence of surface OH groups can decrease the possibility of CH$_x$ scission into surface carbon species.[59] Also for the carbon that has been formed, OH groups are thought to be able to eliminate carbon deposition.[52] There are mainly three routes that contribute to carbon deposition in ESR: (i) ethanol dehydration to ethylene (eq 1), followed by polymerization to coke (eq 2); (ii) boudouard reaction (eq 3); (iii) hydrocarbon decomposition (eq 4). The extent of each reaction depends on reaction conditions and catalyst properties. While low reaction temperature and acidic support favor the formation of carbon through reactions 1, 2, and 3, reactions 4 are the main routes for carbon formation at intermediate and high temperatures. Our stability test was performed at 400 and 600 °C (intermediate and high temperatures), and the acidity of the two catalysts were all very weak (Supporting Information Figure S3), so carbon formation is mainly through hydrocarbon decomposition, and carbon deposition was less on Ni/SiO$_{2P}$ compared to that on Ni/SiO$_{2I}$ which is due to the remaining OH groups in Ni/SiO$_{2P}$.

$$C_2H_5OH \rightarrow C_2H_4 + H_2O \qquad (1)$$

$$C_2H_4 \rightarrow coke \qquad (2)$$
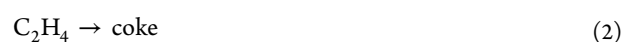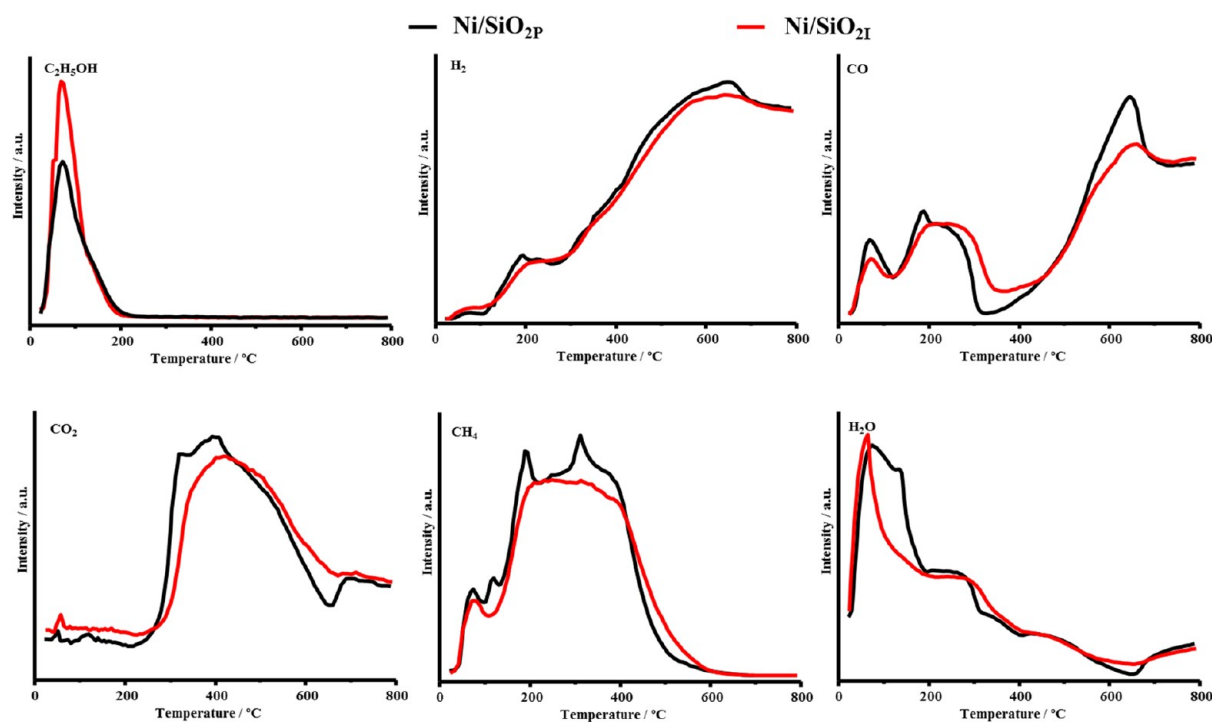
Figure 11. Temperature programmed surface reaction on Ni/SiO_2 catalysts. A mixture containing 0.3 vol% EtOH and 2.4 vol% H_2O in Ar is flown (F = 20 mL/min) in the reactor while temperature is ramped at a linear rate of 10 °C/min; mass of catalyst, 50 mg; P = 1 atm.

$$2CO \rightarrow CO_2 + C \tag{3}$$

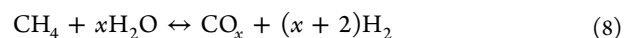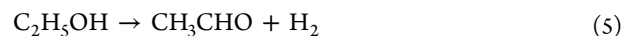$$CH_4 \rightarrow C + 2H_2 \tag{4}$$
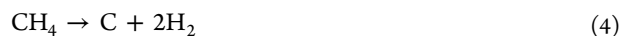
Metallic Ni nanoparticles in the Ni-containing PS are loaded on the surface of the remaining unreduced PS as well as on amorphous silica. The TPR results and TEM images have confirmed that Ni/SiO_{2P} has a stronger metal−support interaction compared to Ni/SiO_{2I}. Che et al. have also found that the interaction between nickel particles and support in Ni-containing PS prepared by a two-step procedure is stronger compared to that in conventional Ni/SiO_2 catalysts prepared by impregnation.[35]

Ni-containing PS consists of a brucite-type sheet containing Ni^{2+} in octahedral coordination and a sheet containing linked tetrahedral SiO_4 units.[35,60] While on reduced Ni/SiO_{2P} catalyst, it is suggested that some of the Ni (II) phase in nickel PS was not reduced (Figures 3 and 4). These ions bonded to the silica surface would probably act as anchoring sites for the metal particles, leading to their stabilization, and favoring the metal dispersion and the resistance to sintering. Several experimental[61,62] and theoretical[63] studies also suggested that unreduced ions at the metal−support interface contribute to the strong metal−support interaction. However, nickel was fully reduced on Ni/SiO_{2I} as can be seen from XRD and TEM results. Consequently, the higher nickel dispersion and stronger metal−support interaction were attained on Ni/SiO_{2P} compared to Ni/SiO_{2I}.

Reaction Analysis. ESR is a complicated process; several reaction mechanisms have been proposed in early work.[64−66] Reaction pathway depends on the active metal of the catalyst. Fatsikostas and Verykios[66] have reported that on nickel-based catalysts ethanol first dehydrogenated into acetaldehyde (eq 5), and then acetaldehyde would crack into CO and CH_4 (eq 6). CO would be converted into CO_2 and H_2 via WGSR (eq 7), while CH_4 can be converted into CO_x and H_2 via methane

steam reforming (eq 8). In this system, nickel mainly promotes C−C and C−H cleavages [reactions 5 and 6]. Nickel particles also have activity in CH_4 and CO transformation [reactions 7 and 8].[49] As both reactions are reversible, products distributions are determined by the availability of types of active sites.

$$C_2H_5OH \rightarrow CH_3CHO + H_2 \tag{5}$$

$$CH_3CHO \rightarrow CO + CH_4 \tag{6}$$

$$CO + H_2O \leftrightarrow CO_2 + H_2 \tag{7}$$

$$CH_4 + xH_2O \leftrightarrow CO_x + (x + 2)H_2 \tag{8}$$

In order to gain preliminary understanding of the reaction pathway, we have carried out TPSR measurements on Ni/SiO_2 catalysts (Figure 11). One can see that ethanol was fully converted after 200 °C on both of the Ni/SiO_2 catalysts. Three H_2 peaks are evolved during the reaction; the first one at ∼100 °C comprised of H_2, CO, and CH_4 peaks could be ascribed to ethanol decomposition.[67] The second hydrogen peak appears around 200−400 °C accompanying with the evolution of CO_2, where CO concentration is low. This is due to the coupling of WGSR and ethanol decomposition,[16,66] which is in good accordance with the low H_2O signal. While the appearance of the CH_4 peak indicates the occurrence of methanation reaction coupled with acetaldehyde decomposition in the same temperature ranges.[50] The third peak at about 600 °C, where the highest H_2 and CO peak and the lowest H_2O and CH_4 signal were also observed, is due to the methane and ethanol steam reforming reactions. The results suggest that at intermediate and high temperatures (400−700 °C) hydrogen production rate is higher on Ni/SiO_{2P} compared to that on Ni/SiO_{2I}, which agrees well with the results under steady reaction conditions. In all cases, the evolution of CH_4, CO, and CO_2 is observed in the same temperature range. However, the CO

Scheme 2. Proposed Reaction Scheme on Ni/SiO₂P
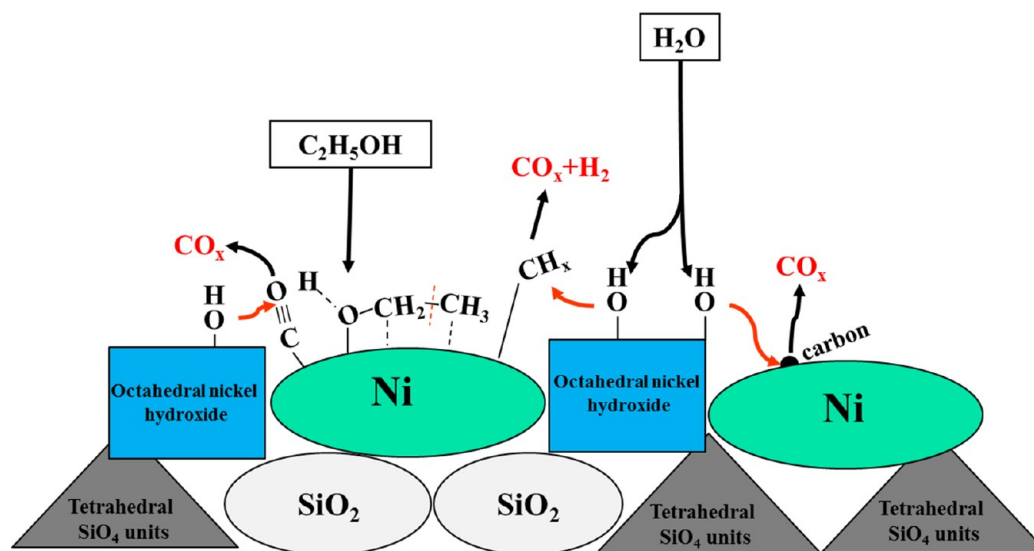
concentration of Ni/SiO$_{2P}$ in the second peak range is lower than that of Ni/SiO$_{2I}$, whereas the inverse trend can be seen for CH$_4$, implying that Ni/SiO$_{2P}$ has a higher WGSR and methanation reactivity compared to Ni/SiO$_{2I}$. In the high temperature range (500−700 °C), H$_2$ and CO concentration are both higher on Ni/SiO$_{2P}$ compared to Ni/SiO$_{2I}$, implying a higher ethanol steam reforming reactivity on Ni/SiO$_{2P}$.

The ESR reactivity is closely dependent on nickel dispersion; high dispersion of nickel is favorable for ethanol conversion and H$_2$ selectivity.[55,68] In our system, Ni/SiO$_{2P}$ has higher TOF and H$_2$ selectivity from 400 to 700 °C compared to Ni/SiO$_{2I}$ (Figure 5), consistent with the higher nickel dispersion of Ni/SiO$_{2P}$. Since nickel has low ability to activate water,[69] water is usually activated over the support. XRD patterns and IR results proved that the PS structure remains partially intact with surface OH groups in the reduced Ni/SiO$_{2P}$ catalyst, which would facilitate the activation of water. The argument has also been supported by Kermarec et al.[39] that the OH band in PS structure is sensitive to hydrogen bonding with interlayer water molecules.

Catalyst deactivation in steam reforming is usually caused by the loss of nickel dispersion via carbon deposition and nickel sintering.[24,70,71] Frusteri et al. have investigated the performance of MgO-supported Pd, Rh, Ni, and Co catalysts in ESR.[72] TEM images of fresh and used catalysts revealed pronounced metal sintering for Pd, Ni, and Co. Calles et al. have found a severe deactivation on Cu−Ni/SBA-15 catalyst from carbon deposition and have reduced it by Ce or La modification.[73] The authors correlated the deactivation of the catalyst to carbon deposition, since nickel particle size on Ni/SiO$_{2P}$ increased little after 30 and 60 h reaction, and the nickel particle size of Ni/SiO$_{2I}$ decreased much. Severe carbon deposition on Ni/SiO$_{2I}$ leading to the gradual loss of reactivity has been approved by TG and TEM results. Comparatively, the PS structure in Ni/SiO$_{2P}$ has a stronger metal−support interaction and a better nickel dispersion compared to Ni/SiO$_{2I}$, accounting for the improved reactivity and stability. Additionally, the remaining OH groups in the partly reduced Ni-containing PS is favorable for eliminating carbon deposition,[41] which could be the origin of enhanced stability on Ni/SiO$_{2P}$.

On the basis of our results and general understanding of the literature, we have proposed a reaction cartoon scheme of ESR on Ni/SiO$_{2P}$ (Scheme 2). In the presence of nickel, the first key reaction should be the dehydrogenation of ethanol to surface adsorbed CH$_3$CH$_2$O$_{ads}$. As Yates and co-workers have shown,[21] metallic nickel particles cause bond breaking of an ethanol molecule in the following order: O—H, —CH$_2$—, C—C, and —CH$_3$. Therefore, the following scheme should be the transformation of CH$_3$CH$_2$O$_{ads}$, and the C—C bond cleavage to produce adsorbed C≡O and CH$_x$ on the nickel surface. Since OH groups are present in the partially reduced phyllosilicates, they would oxidize C≡O and CH$_x$ to form H$_2$ and CO$_x$,[52] while water would chemisorb on octahedral nickel oxide, replenishing the OH groups in the phyllosilicates.[41] Subsequently, the intermediate products can be fully converted to CO$_2$ and H$_2$. Detailed in situ IR and TPRS measurements are underway to further understand the reaction pathway of our Ni/SiO$_{2P}$ catalysts.

■ CONCLUSIONS

We have shown that the Ni-containing PS with layered structure can be obtained via the conventional AE method. The prepared phyllosilicate catalysts have several characters: (1) unique layered structure; (2) presence of Ni(OH)$_2$ in the reduced catalysts; and (3) enhanced binding of Ni species. These properties contribute to the stronger metal−support interaction and higher nickel dispersion compared to Ni/SiO$_{2I}$, which accounts for the improved reactivity and stability of the Ni/SiO$_2$ catalyst on ESR. Remaining OH groups on Ni/SiO$_{2P}$ upon the reduction facilitate elimination of carbon species deposited during the reaction. The severe carbon deposition induces Ni$_3$C formation, thus leading to the reconstruction of nickel particles and deactivation of the Ni/SiO$_{2I}$ catalyst. We have also proposed a reaction scheme on Ni/SiO$_{2P}$ reflecting that the effect of PS structure on the reaction pathways. However, we need to point out the amount of remained PS structure in the reduced Ni/SiO$_{2P}$ cannot be tuned in a controllable manner based on the preparation method we employed, and thus further improvement on the synthetic method of catalysts would be desirable.

■ ASSOCIATED CONTENT

Ⓢ Supporting Information

N₂ adsorption−desorption isotherms, pore size distribution, TG/DTG profiles, and NH₃-TPD profiles of the catalysts. This material is available free of charge via the Internet at http://pubs.acs.org.

■ AUTHOR INFORMATION

Corresponding Author

*E-mail: jlgong@tju.edu.cn. Fax: +86-22-87401818.

Notes

The authors declare no competing financial interest.

■ ACKNOWLEDGMENTS

■ REFERENCES

(1) Navarro, R. M.; Peña, M. A.; Fierro, J. L. G. Hydrogen Production Reactions from Carbon Feedstocks: Fossil Fuels and Biomass. *Chem. Rev.* **2007**, *107* (10), 3952−3991.

(2) Norskov, J. K.; Christensen, C. H. Toward Efficient Hydrogen Production at Surfaces. *Science* **2006**, *312* (5778), 1322−1323.

(3) Chheda, J. N.; Huber, G. W.; Dumesic, J. A. Liquid-Phase Catalytic Processing of Biomass-Derived Oxygenated Hydrocarbons to Fuels and Chemicals. *Angew. Chem., Int. Ed.* **2007**, *46* (38), 7164−7183.

(4) Haryanto, A.; Fernando, S.; Murali, N.; Adhikari, S. Current status of hydrogen production techniques by steam reforming of ethanol: A review. *Energ Fuel* **2005**, *19* (5), 2098−2106.

(5) Deluga, G. A.; Salge, J. R.; Schmidt, L. D.; Verykios, X. E. Renewable Hydrogen from Ethanol by Autothermal Reforming. *Science* **2004**, *303* (5660), 993−997.

(6) Turner, J. A. Sustainable Hydrogen Production. *Science* **2004**, *305* (5686), 972−974.

(7) Cortright, R. D.; Davda, R. R.; Dumesic, J. A. Hydrogen from catalytic reforming of biomass-derived hydrocarbons in liquid water. *Nature* **2002**, *418* (6901), 964−967.

(8) Bion, N.; Duprez, D.; Epron, F. Design of nanocatalysts for green hydrogen production from bioethanol. *ChemSusChem* **2012**, *5* (1), 76−84.

(9) Wang, W.; Wang, Y. Q. Thermodynamic analysis of steam reforming of ethanol for hydrogen generation. *Int. J. Energy Res.* **2008**, *32* (15), 1432−1443.

(10) Ni, M.; Leung, D. Y. C.; Leung, M. K. H. A review on reforming bio-ethanol for hydrogen production. *Int. J. Hydrogen Energy* **2007**, *32* (15), 3238−3247.

(11) Vaidya, P. D.; Rodrigues, A. E. Insight into steam reforming of ethanol to produce hydrogen for fuel cells. *Chem. Eng. J.* **2006**, *117* (1), 39−49.

(12) Eberle, U.; Felderhoff, M.; Schüth, F. Chemical and Physical Solutions for Hydrogen Storage. *Angew. Chem., Int. Ed.* **2009**, *48* (36), 6608−6630.

(13) Llorca, J.; Homs, N.; Ramirez de la Piscina, P. In situ DRIFT-mass spectrometry study of the ethanol steam-reforming reaction over carbonyl-derived Co/ZnO catalysts. *J. Catal.* **2004**, *227* (2), 556−560.

(14) Matsumura, Y.; Ishibe, H. Suppression of CO by-production in steam reforming of methanol by addition of zinc oxide to silica-supported copper catalyst. *J. Catal.* **2009**, *268* (2), 282−289.

(15) Song, H.; Ozkan, U. S. Ethanol steam reforming over Co-based catalysts: Role of oxygen mobility. *J. Catal.* **2009**, *261* (1), 66−74.

(16) Sanchez-Sanchez, M. C.; Yerga, R. M. N.; Kondarides, D. I.; Verykios, X. E.; Fierro, J. L. G. Mechanistic Aspects of the Ethanol Steam Reforming Reaction for Hydrogen Production on Pt, Ni, and PtNi Catalysts Supported on gamma-Al₂O₃. *J. Phys. Chem. A* **2010**, *114* (11), 3873−3882.

(17) Aupretre, F.; Descorme, C.; Duprez, D.; Casanave, D.; Uzio, D. Ethanol steam reforming over MgₓNi₁₋ₓAl₂O₃ spinel oxide-supported Rh catalysts. *J. Catal.* **2005**, *233* (2), 464−477.

(18) Can, F.; Le Valant, A.; Bion, N.; Epron, F.; Duprez, D. New active and selective Rh-ReOₓ-Al₂O₃ catalysts for ethanol steam reforming. *J. Phys. Chem. C* **2008**, *112* (36), 14145−14153.

(19) Jacobs, G.; Keogh, R. A.; Davis, B. H. Steam reforming of ethanol over Pt/ceria with co-fed hydrogen. *J. Catal.* **2007**, *245* (2), 326−337.

(20) Zhang, C.; Li, S.; Li, M.; Wang, S.; Ma, X.; Gong, J. Enhanced oxygen mobility and reactivity for ethanol steam reforming. *AIChE J.* **2012**, *58* (2), 516−525.

(21) Gates, S. M.; Russell, J. N., Jr; Yates, J. T., Jr Bond activation sequence observed in the chemisorption and surface reaction of ethanol on Ni(111). *Surf. Sci.* **1986**, *171* (1), 111−134.

(22) Xu, J.; Zhang, X.; Zenobi, R.; Yoshinobu, J.; Xu, Z.; Yates, J. T., Jr Ethanol decomposition on Ni(111): observation of ethoxy formation by IRAS and other methods. *Surf. Sci.* **1991**, *256* (3), 288−300.

(23) Zhang, C.; Zhang, P.; Li, S.; Wu, G.; Ma, X.; Gong, J. Superior reactivity of skeletal Ni-based catalysts for low-temperature steam reforming to produce CO-free hydrogen. *Phys. Chem. Chem. Phys.* **2012**, *14* (10), 3295−8.

(24) Sehested, J. Four challenges for nickel steam-reforming catalysts. *Catal. Today* **2006**, *111* (1−2), 103−110.

(25) Liu, C.-j.; Ye, J.; Jiang, J.; Pan, Y. Progresses in the Preparation of Coke Resistant Ni-based Catalyst for Steam and CO₂ Reforming of Methane. *ChemCatChem* **2011**, *3* (3), 529−541.

(26) Bezemer, G.; Radstake, P.; Koot, V.; Vandillen, A.; Geus, J.; Dejong, K. Preparation of Fischer−Tropsch cobalt catalysts supported on carbon nanofibers and silica using homogeneous deposition-precipitation. *J. Catal.* **2006**, *237* (2), 291−302.

(27) Li, M.; Wang, X.; Li, S.; Wang, S.; Ma, X. Hydrogen production from ethanol steam reforming over nickel based catalyst derived from Ni/Mg/Al hydrotalcite-like compounds. *Int. J. Hydrogen Energ.* **2010**, *35* (13), 6699−6708.

(28) Busca, G.; Costantino, U.; Montanari, T.; Ramis, G.; Resini, C.; Sisani, M. Nickel versus cobalt catalysts for hydrogen production by ethanol steam reforming: Ni-Co-Zn-Al catalysts from hydrotalcite-like precursors. *Int. J. Hydrogen Energ.* **2010**, *35* (11), 5356−5366.

(29) Yu, X.-P.; Chu, W.; Wang, N.; Ma, F. Hydrogen Production by Ethanol Steam Reforming on NiCuMgAl Catalysts Derived from Hydrotalcite-Like Precursors. *Catal. Lett.* **2011**, 1−9.

(30) Natile, M. M.; Poletto, F.; Galenda, A.; Glisenti, A.; Montini, T.; Rogatis, L. D.; Fornasiero, P. La₀.₆Sr₀.₄Co₁₋ᵧFeᵧO₃₋δ Perovskites: Influence of the Co/Fe Atomic Ratio on Properties and Catalytic Activity toward Alcohol Steam-Reforming. *Chem. Mater.* **2008**, *20* (6), 2314−2327.

(31) Urasaki, K.; Tokunaga, K.; Sekine, Y.; Matsukata, M.; Kikuchi, E. Production of hydrogen by steam reforming of ethanol over cobalt and nickel catalysts supported on perovskite-type oxides. *Catal. Commun.* **2008**, *9* (5), 600−604.

(32) Urasaki, K.; Sekine, Y.; Kawabe, S.; Kikuchi, E.; Matsukata, M. Catalytic activities and coking resistance of Ni/perovskites in steam reforming of methane. *Appl. Catal., A* **2005**, *286* (1), 23−29.

(33) Peña, M. A.; Fierro, J. L. G. Chemical Structures and Performance of Perovskite Oxides. *Chem. Rev.* **2001**, *101* (7), 1981−2018.

(34) Burattin, P.; Che, M.; Louis, C. Ni/SiO₂ Materials Prepared by Deposition−Precipitation: Influence of the Reduction Conditions and Mechanism of Formation of Metal Particles. *J. Phys. Chem. B* **2000**, *104* (45), 10482−10489.

(35) Che, M.; Cheng, Z. X.; Louis, C. Nucleation and Particle Growth Processes Involved in the Preparation of Silica-Supported

171

dx.doi.org/10.1021/sc300081q | *ACS Sustainable Chem. Eng.* 2013, 1, 161−173

Nickel Materials by a Two-Step Procedure. *J. Am. Chem. Soc.* **1995**, *117* (7), 2008−2018.

(36) Carriat, J. Y.; Che, M.; Kermarec, M.; Verdaguer, M.; Michalowicz, A. Control of Dispersion of Ni^{2+} Ions via Chelate Ligands in the Preparation of Ni/SiO$_2$ Materials. A XAFS Study. *J. Am. Chem. Soc.* **1998**, *120* (9), 2059−2070.

(37) Burattin, P.; Che, M.; Louis, C. Metal Particle Size in Ni/SiO$_2$ Materials Prepared by Deposition−Precipitation: Influence of the Nature of the Ni(II) Phase and of Its Interaction with the Support. *J. Phys. Chem. B* **1999**, *103* (30), 6171−6178.

(38) Sietsma, J. R. A.; Meeldijk, J. D.; Versluijs-Helder, M.; Broersma, A.; Dillen, A. J. v.; de Jongh, P. E.; de Jong, K. P. Ordered Mesoporous Silica to Study the Preparation of Ni/SiO$_2$ ex Nitrate Catalysts: Impregnation, Drying, and Thermal Treatments. *Chem. Mater.* **2008**, *20* (9), 2921−2931.

(39) Kermarec, M.; Carriat, J. Y.; Burattin, P.; Che, M.; Decarreau, A. FTIR Identification of the Supported Phases Produced in the Preparation of Silica-Supported Nickel Catalysts. *J. Phys. Chem.* **1994**, *98* (46), 12008−12017.

(40) Bartholomew, C. H.; Pannell, R. B. The stoichiometry of hydrogen and carbon monoxide chemisorption on alumina- and silica-supported nickel. *J. Catal.* **1980**, *65* (2), 390−401.

(41) Sivaiah, M. V.; Petit, S.; Barrault, J.; Batiot-Dupeyrat, C.; Valange, S. CO$_2$ reforming of CH$_4$ over Ni-containing phyllosilicates as catalyst precursors. *Catal. Today* **2010**, *157* (1−4), 397−403.

(42) Melo, M. A., Jr; Airoldi, C. Energetic features of copper and lead sorption by innovative aminoalcohol-functionalized cobalt phyllosilicates. *Dalton Trans.* **2010**, *39* (42), 10217−10227.

(43) Burattin, P.; Che, M.; Louis, C. Molecular Approach to the Mechanism of Deposition−Precipitation of the Ni(II) Phase on Silica. *J. Phys. Chem. B* **1998**, *102* (15), 2722−2732.

(44) Clause, O.; Bonneviot, L.; Che, M. Effect of the preparation method on the thermal stability of silica-supported nickel oxide as studied by EXAFS and TPR techniques. *J. Catal.* **1992**, *138* (1), 195−205.

(45) Sun, K. Q.; Marceau, E.; Che, M. Evolution of nickel speciation during preparation of Ni-SiO$_2$ catalysts: effect of the number of chelating ligands in $[Ni(en)_x(H_2O)_{6−2x}]^{2+}$ precursor complexes. *Phys. Chem. Chem. Phys.* **2006**, *8* (14), 1731−8.

(46) Sivaiah, M. V.; Petit, S.; Beaufort, M. F.; Eyidi, D.; Barrault, J.; Batiot-Dupeyrat, C.; Valange, S. Nickel based catalysts derived from hydrothermally synthesized 1:1 and 2:1 phyllosilicates as precursors for carbon dioxide reforming of methane. *Micropor. Mesopor. Mat.* **2011**, *140* (1−3), 69−80.

(47) Lin, J.-H.; Guliants, V. V. Hydrogen Production through Water−Gas Shift Reaction over Supported Cu, Ni, and Cu−Ni Nanoparticle Catalysts Prepared from Metal Colloids. *ChemCatChem* **2012**, *4* (10), 1611−1621.

(48) Kim, S. H.; Nam, S.-W.; Lim, T.-H.; Lee, H.-I. Effect of pretreatment on the activity of Ni catalyst for CO removal reaction by water−gas shift and methanation. *Appl. Catal., B* **2008**, *81* (1−2), 97−104.

(49) Li, S.; Li, M.; Zhang, C.; Wang, S.; Ma, X.; Gong, J. Steam reforming of ethanol over Ni/ZrO$_2$ catalysts: Effect of support on product distribution. *Int. J. Hydrogen Energy* **2012**, *37* (3), 2940−2949.

(50) de Lima, S. M.; da Silva, A. M.; da Costa, L. O. O.; Graham, U. M.; Jacobs, G.; Davis, B. H.; Mattos, L. V.; Noronha, F. B. Study of catalyst deactivation and reaction mechanism of steam reforming, partial oxidation, and oxidative steam reforming of ethanol over Co/CeO$_2$ catalyst. *J. Catal.* **2009**, *268* (2), 268−281.

(51) Alstrup, I. A new model explaining carbon filament growth on nickel, iron, and Ni−Cu alloy catalysts. *J. Catal.* **1988**, *109* (2), 241−251.

(52) Bartholomew, C. H. Carbon deposition in steam reforming and methanation. *Catal. Rev.−Sci. Eng.* **1982**, *24* (1), 67−112.

(53) Czekaj, I.; Loviat, F.; Raimondi, F.; Wambach, J.; Biollaz, S.; Wokaun, A. Characterization of surface processes at the Ni-based catalyst during the methanation of biomass-derived synthesis gas: X-

ray photoelectron spectroscopy (XPS). *Appl. Catal., A* **2007**, *329*, 68−78.

(54) Sinharoy, S.; Levenson, L. L. The formation and decomposition of nickel carbide in evaporated nickel films on graphite. *Thin Solid Films* **1978**, *53* (1), 31−36.

(55) Li, M.; Li, S.; Zhang, C.; Wang, S.; Ma, X.; Gong, J. Ethanol steam reforming over Ni/Ni$_x$Mg$_{1-x}$O: Inhibition of surface nickel species diffusion into the bulk. *Int. J. Hydrogen Energy* **2010**, *36* (1), 326−332.

(56) Turlier, P.; Praliaud, H.; Moral, P.; Martin, G. A.; Dalmon, J. A. Influence of the nature of the support on the reducibility and catalytic properties of nickel: evidence for a new type of metal support interaction. *Appl. Catal.* **1985**, *19* (2), 287−300.

(57) Verhaak, M. J. F. M.; van Dillen, A. J.; Geus, J. W. Measuring the acid-base properties of supported nickel catalysts using temperature-programmed desorption of ammonia. *Appl. Catal., A* **1993**, *105* (2), 251−269.

(58) Arai, M.; Guo, S.-L.; Nishiyama, Y. Importance of surface hydroxyl groups to the dispersion of nickel impregnated on silica gels. *J. Catal.* **1992**, *135* (2), 638−641.

(59) Wang, S.-G.; Cao, D.-B.; Li, Y.-W.; Wang, J.; Jiao, H. Reactivity of surface OH in CH$_4$ reforming reactions on Ni(111): A density functional theory calculation. *Surf. Sci.* **2009**, *603* (16), 2600−2606.

(60) da Fonseca, M. G.; Silva, C. R.; Barone, J. S.; Airoldi, C. Layered hybrid nickel phyllosilicates and reactivity of the gallery space. *J. Mater. Chem.* **2000**, *10* (3), 789−795.

(61) Haberlandt, H.; Ritschl, F. Quantum chemical investigation of support-metal interactions and their influence on chemisorption. 2. Strong metal-support interaction in H...Ni-MOx (M = titanium, silicon). *J. Phys. Chem.* **1986**, *90* (18), 4322−4330.

(62) Huizinga, T.; Prins, R. ESR investigations of platinum supported on alumina and titania. *J. Phys. Chem.* **1983**, *87* (1), 173−176.

(63) Che, M.; Masure, D.; Chaquin, P. Theoretical study of the formation of oxide-supported metal particles: strength of the chemical glue as represented by transition metal ions at the metal-oxide interface. *J. Phys. Chem.* **1993**, *97* (35), 9022−9027.

(64) Song, H.; Zhang, L.; Ozkan, U. S. Investigation of the Reaction Network in Ethanol Steam Reforming over Supported Cobalt Catalysts. *Ind. Eng. Chem. Res.* **2010**, *49* (19), 8984−8989.

(65) Lu, P.-J.; Chen, T.-S.; Chern, J.-M. Reaction network and kinetic analysis of ethanol steam reforming over a Ru/Al$_2$O$_3$ catalyst. *Catal. Today* **2011**, *174* (1), 17−24.

(66) Fatsikostas, A.; Verykios, X. E. Reaction network of steam reforming of ethanol over Ni-based catalysts. *J. Catal.* **2004**, *225* (2), 439−452.

(67) Padilla, R.; Benito, M.; Rodríguez, L.; Serrano, A.; Muñoz, G.; Daza, L. Nickel and cobalt as active phase on supported zirconia catalysts for bio-ethanol reforming: Influence of the reaction mechanism on catalysts performance. *Int. J. Hydrogen Energy* **2010**, *35* (17), 8921−8928.

(68) Pirez, C.; Capron, M.; Jobic, H.; Dumeignil, F.; Jalowiecki-Duhamel, L. Highly Efficient and Stable CeNiH$_Z$O$_Y$ Nano-Oxyhydride Catalyst for H$_2$ Production from Ethanol at Room Temperature. *Angew. Chem., Int. Ed.* **2011**, *50* (43), 10193−7.

(69) Comas, J.; Mariño, F.; Laborde, M.; Amadeo, N. Bio-ethanol steam reforming on Ni/Al$_2$O$_3$ catalyst. *Chem. Eng. J.* **2004**, *98* (1−2), 61−68.

(70) Trimm, D. L. Coke formation and minimisation during steam reforming reactions. *Catal. Today* **1997**, *37* (3), 233−238.

(71) Bengaard, H. S.; Nørskov, J. K.; Sehested, J.; Clausen, B. S.; Nielsen, L. P.; Molenbroek, A. M.; Rostrup-Nielsen, J. R. Steam Reforming and Graphite Formation on Ni Catalysts. *J. Catal.* **2002**, *209* (2), 365−384.

(72) Frusteri, F.; Freni, S.; Spadaro, L.; Chiodo, V.; Bonura, G.; Donato, S.; Cavallaro, S. H2 production for MC fuel cell by steam reforming of ethanol over MgO supported Pd, Rh, Ni and Co catalysts. *Catal. Commun.* **2004**, *5* (10), 611−615.

(73) Calles, J. A.; Carrero, A.; Vizcaino, A. J. Ce and La modification of mesoporous Cu-Ni/SBA-15 catalysts for hydrogen production

through ethanol steam reforming. *Microporous Mesoporous Mater.* **2009**, *119* (1−3), 200−207.

173

dx.doi.org/10.1021/sc300081q | *ACS Sustainable Chem. Eng.* 2013, 1, 161−173